Available online at www.sciencedirect.com

ScienceDirect

Procedia Structural Integrity 28 (2020) 1520–1535

Structural Integrity Procedia

www.elsevier.com/locate/procedia

1st Virtual European Conference on Fracture

Predicting crack patterns in SiC-based cladding for LWR applications using peridynamics

Abigael Bamgboye[a], Thomas A. Haynes[1], Mark R. Wenman[a,1]

[a]*Department of Materials and Centre for Nuclear Engineering, Imperial College London, London, SW7 2BP, United Kingdom*

Abstract

SiC continuous fibre reinforced SiC matrix (SiC-SiC) composites are a proposed material for accident tolerant fuel cladding. Thermomechanical models of SiC-based cladding under light water conditions indicate that microcracking in the radial direction of the tubing may lead to a loss of hermicity. SiC-based tubing is known to have anisotropic elastic properties but the effect of this anisotropy have not been incorporated into existing thermomechanical models of clad cracking. This work augments an existing isotropic 2D peridynamic model of cracking and damage in the r-θ plane of a SiC-based cladding to account for the orthotropic elastic properties of SiC-SiC composite tubing. Three SiC-based architectures are modelled under normal operating conditions of a UO_2-fuelled pressurised water reactor (PWR). The results of the anisotropic SiC-cladding model are compared with the results of the isotropic model, and the sensitivity of results to material anisotropy, thermal conductivity, and applied linear power rating are analysed.

The results of this analysis show that anisotropy has a significant effect on the damage and crack patterns observed in the r-θ plane of SiC-based cladding, if either an inner or outer monolith is present. The anisotropic model predicts more cracks in two layer clad with an inner monolith and higher levels of damage in a two layer clad with an outer monolith than the isotropic model. Under normal reactor conditions the outer monolith clad architecture was found to remain hermetic.

Keywords: silicon carbide composites; peridynamics; fracture; accident tolerant fuel cladding; LWR

1. Introduction

Following the 2011 Fukushima Daiichi accident, alternatives to the zirconium-based alloys currently used in light water reactors, (termed accident tolerant fuel (ATF) cladding materials) have been an area of interest for the international fission community. Silicon carbide (SiC) is a potential candidate cladding material due to its desirable material

* Corresponding author.
E-mail address: ab6216@ic.ac.uk (Abigael Bamgboye)

10.1016/j.prostr.2020.10.125

properties including high temperature steam oxidation resistance (which is two orders of magnitude higher than zirconium), high temperature strength, low neutron absorbance, high temperature creep resistance [1, 2, 3] .

In its monolithic ceramic form, SiC is brittle and susceptible to catastrophic failure under the tensile hoop loads that would be experienced under cladding conditions. However, in the form of a ceramic matrix composite, SiC-SiC composites retain all the benefits of SiC, as well as increased toughness arising from their pseudo-ductile deformation processes (matrix microcracking, crack deflection in interphase and fibre pull-out) [4]. One of the current limitations of SiC-SiC is its propensity to undergo microcracking at stresses far below its UTS; microcracking of the matrix occurs at the proportional limit stress (PLS) which varies from 80-180 MPa [2], depending on the composite manufacturing method, porosity and the type of nuclear grade SiC fibres used. Furthermore, thermomechanical models have shown that typical operating conditions in an LWR produce stresses exceeding the PLS of SiC-SiC during reactor shutdown for refuelling outages [5, 6].

As a fully composite cladding design is insufficient to meet hermicity requirements of fuel cladding, various multi-layer cladding architectures featuring chemical vapour deposited SiC monoliths have been proposed [5, 6, 7, 8]. A monolith layer has been proven to provide a gas tight hermetic seal [9], and in a multi-layer cladding architecture, it is proposed that the weaknesses of fully composite and fully monolith SiC can be overcome. In a previous work by Haynes et al., peridynamics was used to model crack patterns in the r-θ plane of SiC-based cladding [10]. This work indicated that cracks formed in a two-layer clad architecture, with an inner monolith, would propagate into the composite, however this model does not incorporate the underlying anisotropy of SiC-SiC tubing [10, 11] which thermomechanical modelling (as performed by Singh et al. [12]) has shown can significantly affect maximum cladding hoop stress. Consequently, this research builds on the work of Haynes et al. [10], and introduces anisotropy in the model, to assess its impact on crack patterns and the implications for cladding hermicity for three SiC-based cladding architectures. The sensitivity of the anisotropic model to mechanical and thermal property inputs (elastic modulus anisotropy and thermal conductivity) and to fuel operating conditions (applied linear power rating) are analysed.

1.1. Thermomechanical Modelling SiC-based cladding

Various groups have used thermo-mechanical analysis techniques including fuel codes to predict the behaviour of SiC-SiC cladding under LWR conditions. Softwares and fuel codes used to date for these analyses include FRAPCON [8], BISON [6, 12], MATLAB [5], ANSYS [5], ADINA [7] and ABAQUS [6, 12]. These analyses have shown that SiC-SiC cladding would experience a moderate tensile hoop stress in the inner region of the clad, with a compressive hoop stress in the outer region of the cladding. Notably, these models predict that the tensile and compressive stresses experienced by the clad increase substantially above the PLS of SiC-SiC during reactor shutdown.

As the above methods show, finite element (FE) analysis works well for modelling the complex stress-state of LWR cladding – however the formulation of FE using spatial derivatives presents a number of challenges for modelling cracking and fracture. The differential equations governing FE models are undefined at discontinuities such as cracks and interfaces [13], hence prior knowledge of the failure mode and crack path must be known so special treatment must be applied at the crack tip [14]. This leads to difficulties in modelling complex dynamic crack interaction including branching and coalescence.

Peridynamics is a continuum mechanics method introduced by Silling in 2000 [15]. It does not suffer from the aforementioned limitations due to its formulation using spatial integrals. Its strengths include being able to model cracks without *a priori* knowledge of their initiation points, its relative ease of modelling crack coalescence and branching, and its ability to model non-local effects (a single point is affected by its neighbourhood of points, rather than solely its immediate neighbours) [16]. Due to these advantages, peridynamics was the preferred method for modelling the microcracking behaviour of a section of SiC-based cladding.

2. Model Description

2.1. Peridynamics Formulation

This work uses bond-based peridynamics, following the formulation of [17]. Each material point experiences a pairwise force from other materials points, x' within a specified volume (3D) or area (2D) called the horizon.

The equation of motion for a material point, x , described by Newton's second law, $F = ma$, is given by:

$$p(x)\,\ddot{u}(x,t) = \int_H f(\eta,\xi)dV_x + b(x,t) \tag{1}$$

where $p(x)$ is the mass density of a material point, V_x is the volume of the material point, $\ddot{u}(x,t)$ is the acceleration, $f(\eta,\xi)$is the force function and $b(x,t)$ is the body force density of the material point located at x, integrated over the horizon, H. η describes the relative displacement of points x and x' in the reference configuration [14]:

$$\eta = u(x',t') - u(x,t) \tag{2}$$

where $u(x,t)$ and $u(x',t')$ are the displacements of the materials points x and x' at time t. ξ is the relative position of the material point during the initial configuration, given by:

$$\xi = x' - x \tag{3}$$

The force function is a function of a micromodulus, c, (representing the stiffness of the bond), a history dependent scalar damage function, μ, and s, the stretch of a bond.

$$f = c\mu s \tag{4}$$

c is obtained by equating the classical strain energy with the peridynamic strain energy density. The micromodulus in the 2D case is given by Equation 5 [18].

$$c_{2D} = \frac{12E}{\pi h \delta^3 (1+\nu)} \tag{5}$$

where E is the elastic modulus, δ is the horizon ratio, h is the plate thickness and ν is the Poisson's ratio. [19].

In the 2D case, there are fixed Poisson's ratios for plane stress and plane strain conditions. As discussed by Trageser et al. [18], the Poisson's ratio constraints are necessary because the peridynamic strain energy density is only equal to the classical strain energy density for two values of ν; when ν = 1/3 for plane stress and 1/4 for plane strain respectively.

The stretch of a bond, s, is given by:

$$s = \frac{|\xi+\eta| - |\xi|}{\xi} \tag{6}$$

The peridynamic condition for brittle fracture is achieved by denoting that a bond has failed when its stretch exceeds a critical stretch s_c, as shown by Figure 1. Above s_c a bond can no longer sustain load, and for stretches < s_c are elastic and reversible.

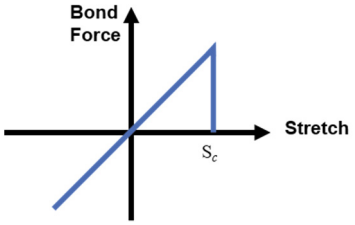

Fig. 1. Schematic showing peridynamic microelastic response.

s_c is calculated from the critical energy release rate, G_c as outlined in Equation 7 [17].

$$s_c = \sqrt{\frac{5G_c}{9k\delta}} \tag{7}$$

μ functions as a way of recording which bonds have not yet exceeded s_c, and are consequently still able to carry load.

$$\mu(\xi, t) = \begin{cases} 1, & if\ s(\xi, t') < s_c, for\ all\ 0 \le t' \le s_c \\ 0, & otherwise \end{cases} \tag{8}$$

2.2. ABAQUS Implementation of Peridynamics

Macek et al. demonstrated that ABAQUS could be used to implement peridynamics [17]. The model presented in this work uses an ABAQUS implementation of peridynamics created by Haynes et al., which builds upon the work of Mella et al. [20, 21]. As in the aforementioned works, material points are represented as nodes, and bonds are represented as trusses. The horizon determines the distance between materials points at which a force-carrying bond can form. As ABAQUS requires some mass to be associated with trusses, thus 99% of the system's mass is captured by the material points, and 1% of the mass is held by the trusses.

$$\rho_{\text{truss}} = 0.001\rho_0 \frac{A}{n\Sigma_i L_i} \tag{9}$$

where A is the area of the truss, ρ_0 is the bulk density, L_i is the length of each truss in the model, and n is the nodal spacing.

The elastic modulus of a truss is given by:

$$E_{\text{truss}} = \frac{c}{A} \tag{10}$$

where c is the micromodulus, and A is the area of the truss. The area of the truss is set to the nodal spacing multiplied by the depth of the sample.

A FORTRAN preprocessor sets whether the model is in pesudo-plane stress or plane strain, the mesh size and the cladding architecture. All nodes are equally spaced apart in a square grid. An input file is used to govern parameters of the simulation; it applies the forces and thermal conditions representing the r-θ plane of an LWR.

In this work, the fibre-pull out region of SiC-SiC deformation is represented by utilising the ABAQUS *PLASTIC key word in a material input file. The plastic strain at the PLS is set to zero, and plastic strain at the UTS is set to the difference between the strain to failure and elastic strain. Hence in the composite region of the model, bonds deform elastically with an initial slope E, until the PLS before undergoing non-elastic deformation with a lower slope until the strain to failure, as shown in Figure 2.

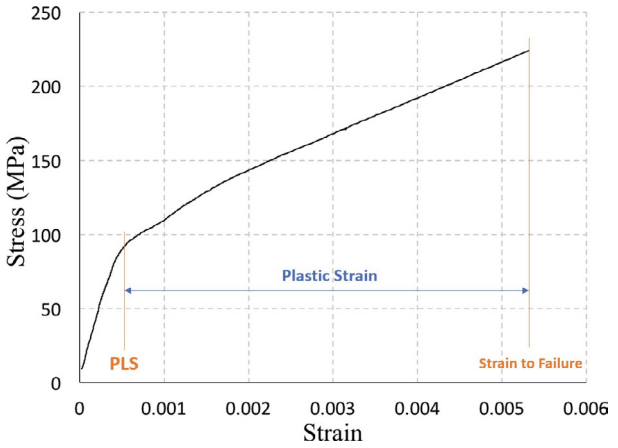

Fig. 2. Typical stress-strain curve for CVD SiC, modified from [22], reproduced under license 4886500589322.

2.3. Incorporation of Anisotropy

In this work, the properties of SiC-SiC are considered macroscopically as shown in Figure 3, hence bonds are not representative of individual fibres. The difference in elastic properties between orthogonal directions is represented by modifying the elastic modulus of a truss, depending on its angle of orientation to the x-axis.

This modification is captured in the user subroutine, USDFLD, through field variable (1), $field(1)$. $field(1)$ is used to apply an edge correction factor to trusses (bonds) in surface regions where less trusses are connected to each node than in the bulk. Without an edge correction factor, these regions would have regions of high compliance and deform prematurely due to having fewer bonds connected to each material point to bear the same load relative to the bulk [19].

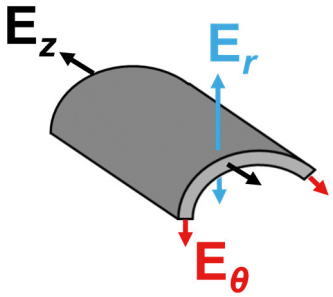

Fig. 3. Schematic to show orthotropic elastic properties of SiC-SiC tubing.

By flattening an 1/8th of a section of tubing and applying boundary conditions to the left and right edges to reflect cladding continuity, we obtain a rectangular specimen where the *x*-axis corresponds to the circumferential direction of cladding, and the *y*-axis refers to the radial direction.

As described in Equation 10, the micromodulus, *c*, is related to the effective elastic constant of the truss. Thus, just as $E_x \neq E_y$, $c_x \neq c_y$ where c_x and c_y are the micromoduli parallel to the *x* and *y*-axis respectively. Hence, *c* is no longer independent of the bond direction, as in the isotropic case, and will have an angular dependence, denoted by $c(\phi)$, where

$$c(\phi) = c_0 \times \mathrm{f}(\phi) \tag{11}$$

where c_0 is the isotropic micromodulus and $\mathrm{f}(\phi)$ is a function with angular dependence.
Let $\alpha = c_y - c_x$, then for $0 \leq \phi \leq \frac{\pi}{2}$:

$$c(\phi) = c_x + \alpha|sin(\phi)| \tag{12}$$

This formulation produces the expected micromodulus when $\phi = 0$ and $\phi = \frac{\pi}{2}$ respectively, however raising the sine term to the power of *N* would also give these results, and series expansions of micromoduli expressions in works by other groups that have implemented anisotropy in peridynamics suggest that index of $N > 1$ is plausible [16]. Thus in benchmarking, different values of *N* were assessed:

$$c(\phi) = c_x + \alpha|sin(\phi)|^N \tag{13}$$

We can relate c_x and c_y using $k = \frac{c_y}{c_x}$. Substituting α with $c_y = kc_x$ gives:

$$c(\phi) = c_x + (kc_x - c_x)|sin(\phi)|^N \tag{14}$$

Factorising this expression with respect to c_x gives:

$$c(\phi) = c_x(1 + k|sin(\phi)|^N - |sin(\phi)|^N) \tag{15}$$

Which simplifies to Equation 16:

$$c(\phi) = c_x(1 + (k-1)|sin(\phi)|^N) \tag{16}$$

From this we can infer that $\mathrm{f}(\phi) = 1 + (k-1)|sin(\phi)|^N$. Thus, in the ABAQUS USDFLD subroutine,

$$field(1)(\phi) = field(1) \times \mathrm{f}(\phi) \tag{17}$$

The angular dependence of the micromodulus is reflected in Figure 4, which illustrates the effective elastic properties of trusses in a peridynamic ABAQUS model.

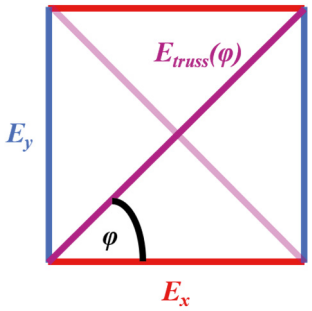

Fig. 4. Schematic to show angular dependence of the trusses' effective elastic modulus.

2.4. Materials Properties

The elastic properties of SiC-SiC tubing are influenced by a number of factors; strength of fibres, interphase material, matrix deposition method, porosity, braiding direction, fibre volume fraction and manufacturing/processing method [3, 12]. The most significant of these factors are fibre braiding angle and fibre strength as they govern the elastic moduli in each of the orthogonal directions [5,12].

Across literature, SiC-SiC composites manufactured from Hi-Nicalon (HNS) SiC fibres with a chemical vapour deposited matrix (CVI SiC-SiC) and a pyrolytical carbon interphase are the most widely explored in experimental conditions application to an LWR reactor [3, 22, 23]. However, limited data exists on the orthotropic pseudo-ductile properties of SiC-SiC, particularly in the radial direction. Singh et al. measured the orthotropic elastic properties of HNS CVI SiC-SI made of a triaxial braid with fibre tow bundles at $\pm 55^o$ and 0^o orientation using resonant ultrasound spectroscopy (RUS). The elastic properties measured using this method are shown in Table 1 [22] and the PLS and UTS properties described in Table 1, with the PLS and UTS data derived from C-ring tests by Jacobsen et al. [11].

Table 1. Properties of Composite Modelled under LWR conditions.

Model	Elastic Moduli (GPa)	Stress at PLS (MPa)	UTS (MPa)	Strain at UTS
Isotropic	248.8	124.4	282	0.0046
Anisotropic	E_x = 248.8, E_y = 79.9	124.4	282	0.0046

In this work, the effect of the irradiation is considered. Studies by Katoh et al. indicate that there is no significant difference in the magnitude of swelling between CVD SiC and CVI SiC-SiC, hence swelling between 200 and 800^{o}C can be described by Equation 18, for SiC-SiC composites made from both HNS and SA3 fibres [24] with swelling saturation at 1 dpa:

$$S = S_c\left(1 - e^{-\frac{\gamma}{\gamma_c}}\right)^{\frac{2}{3}} \tag{18}$$

The temperature dependent thermal expansion behaviour ($125 \leq T \leq 1273$K) of the CVD SiC and HNS SiC-SiC is described by Equation 19 [25]:

$$\alpha = -1.8276 + 0.0178T - 1.5544 \times 10^{-5}T^2 + 4.5246 \times 10^{-9}T^3 \quad (19)$$

Thermal conductivity is described by:

$$\frac{1}{k_{irr}} = \frac{1}{k_0} + \frac{1}{k_{rd}} \quad (20)$$

where k_{irr} is the thermal resistivitiy of the irradiated material, k_0 is the thermal resistivity of the unirradiated material and $k_{rd}$is radiation defect thermal resistivity. This effect saturates within 1 dpa because $\frac{1}{k_{rd}}$ is proportional to swelling [12].

2.5. Cladding Architecture

Three cladding architectures were simulated; a pure composite cladding, a composite cladding with an outer monolith, and a composite cladding with an inner monolith. Where a monolith was present, 1/3 of the cladding width was the monolith [10] as shown in Figure 5. The anisotropic response was applied to the composite region only, and the monolith region continued to retain isotropic properties.

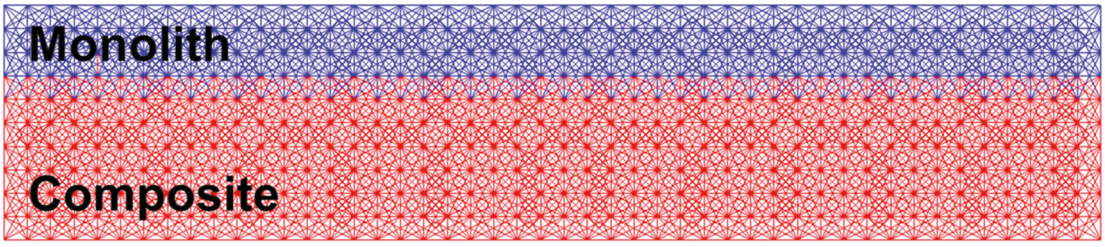

Fig. 5. Model mesh showing isotropic monolith (blue) and anisotropic composite (red) corresponding to a duplex clad with an outer monolith.

CVD SiC manufactured by Rohm and Haas, described in Table 2, was used to represent the monolith material in the simulation of clad under reactor conditions. This material has the typical properties of CVD SiC, with a low coefficient of thermal expansion, high strength, high oxidation resistance and has been used in experiments as a proxy for the SiC-SiC matrix material [26].

Table 2. CVD SiC Properties used to represent thte monolith.

Manufacturer & Sample Name	E (GPa)	ν	Density (kg cm^{-3})
Rohm and Haas CVD SiC	460	0.21	3.21×10^{-3}

2.6. Boundary Conditions | Modelling Clad Performance Under LWR Conditions

The conditions simulated were the typical operating conditions of a PWR undergoing two 18-month fuel cycles and a refuelling cycle, as show in Figure 6. This emulates the work of Haynes et al. with a linear power of 18 kW m^{-1}, and coolant pressure of 15.5 MPa [10].

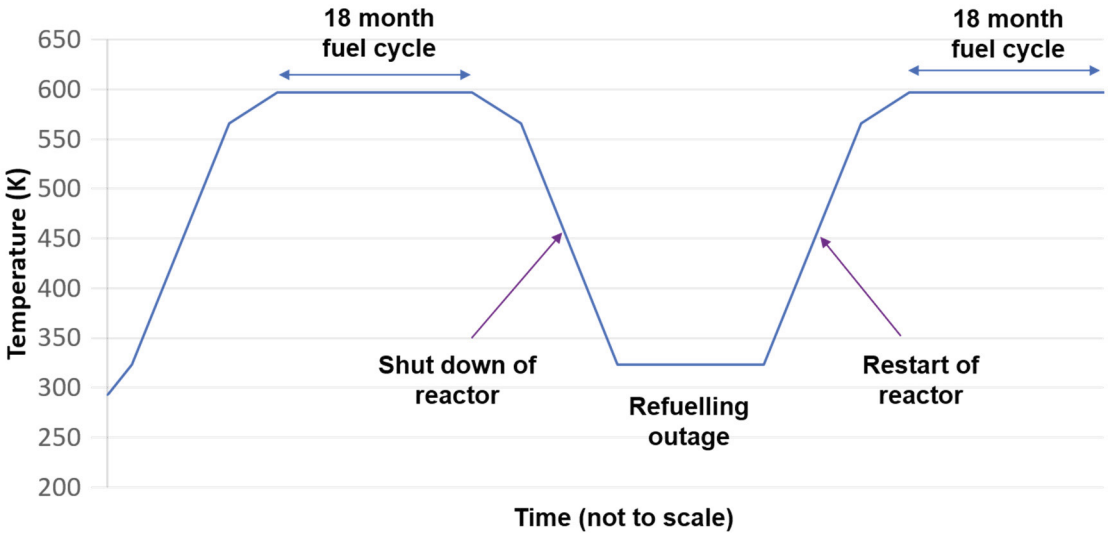

Fig. 6. PWR routine operation cycle - 2x 18 month cycles and a refuelling outage.

3. Results

All data presented were taken at the end of the simulation of reaction operation described in Figure 6, for pseudo-plane strain peridynamic models.

Under the conditions described in Section 2.6, cracking and damage was found to have occurred during the cooling of the reactor before and after refuelling. For the fully composite architecture (with no monolith was present), no broken bonds, or fibre pull-out damage were observed, so the model outputs are not reported.

For the inner monolith architecture as depicted in Figure 7a and 7b, cracks are seen in both the isotropic and anisotropic model. These cracks extend from the inner surface of the clad to the monolith composite interface where they are arrested and do not continue into the composite. The anisotropic model shows some rendering defects at the composite-monolith interface, identifiable by their consistent patterning (circled in Figure 7b). These have arisen because of ABAQUS' method of interpolating the truss values from the surrounding nodes. As seen in Figure 7a, the isotropic model's cracks are straight, while Figure 7b shows cracks predicted by the anisotropic model are slanted, with crack branching occurring. Since monolithic SiC does not contain any fibres, no fibre pull-out response is seen on the monolith region. Fibre pull-out is seen in the composite region of both the isotropic and anisotropic models that include an inner monolith.

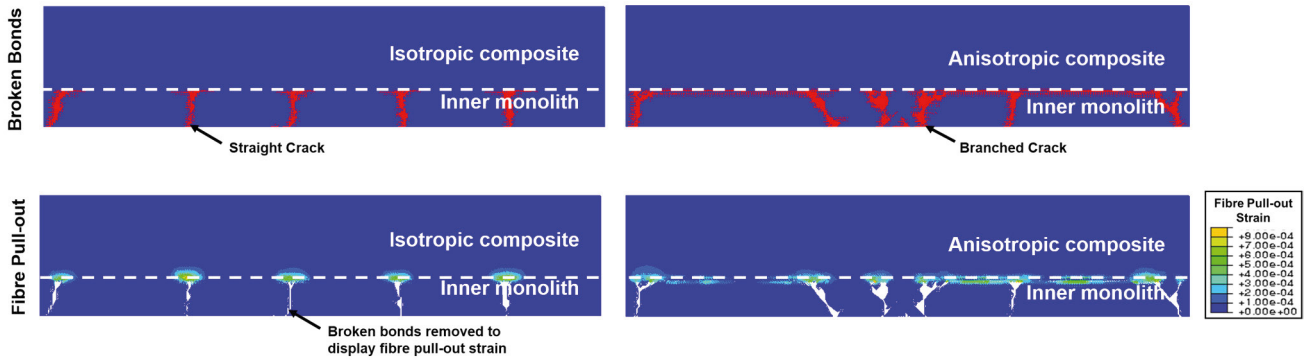

a) Isotropic Model b) Anisotropic Model

Fig. 7. Broken bonds (red) and fibre pull-out strain (key to right) seen in duplex inner monolith peridynamic model under LWR conditions with 0.016 mm node spacing, with some ABAQUS rendering defects seen at monolith-composite interface of anisotropic model (in circled regions).

Figure 8a and Figure 8b show the isotropic and anisotropic model results for an outer monolith duplex clad. Both models indicate minor damage in the outer monolith, though the anisotropic model shows more damage than the isotropic model, as shown by the higher number of broken bonds. Fibre pull-out damage is seen in the composite on the inner surface of the clad, with higher levels of fibre pull-out seen in the anisotropic model. The results obtained under plane stress conditions (not depicted) displayed similar trends as the above plane strain models.

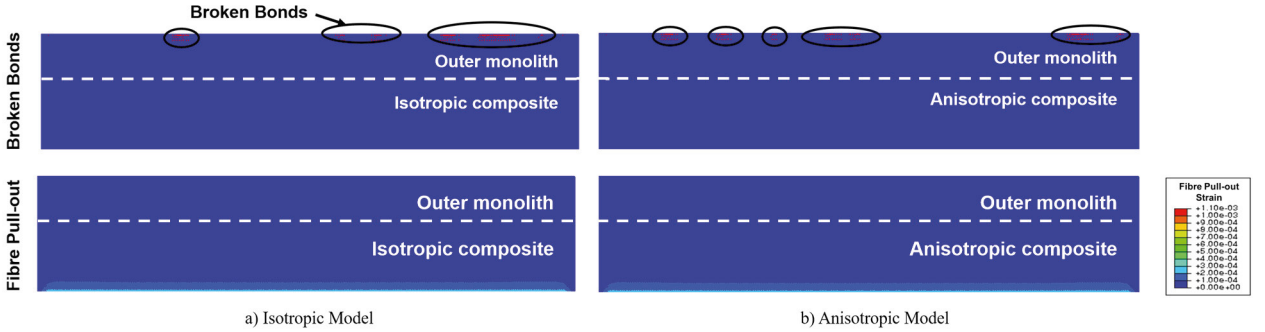

a) Isotropic Model b) Anisotropic Model

Fig. 8. Broken bonds (red) and fibre pull-out strain (key to the right) seen in duplex outer monolith peridynamic model under LWR conditions using 0.016 mm node spacing. Greater amounts of damage were observed in the outer monolith of anisotropic model.

Effect of Level of Elastic Anisotropy

The more non-equal the E_x: E_y ratio of the composite, the higher the number of broken bonds seen in the duplex anisotropic models. As shown in Figure 9, the inner monolith model was much more sensitive to E_x: E_y ratio, than the outer monolith duplex model. The highest ratio tested (3:1) was formulated using the elastic properties measured from RUS experiments by Singh et al., and resulted in significantly more broken bonds for the outer monolith model.

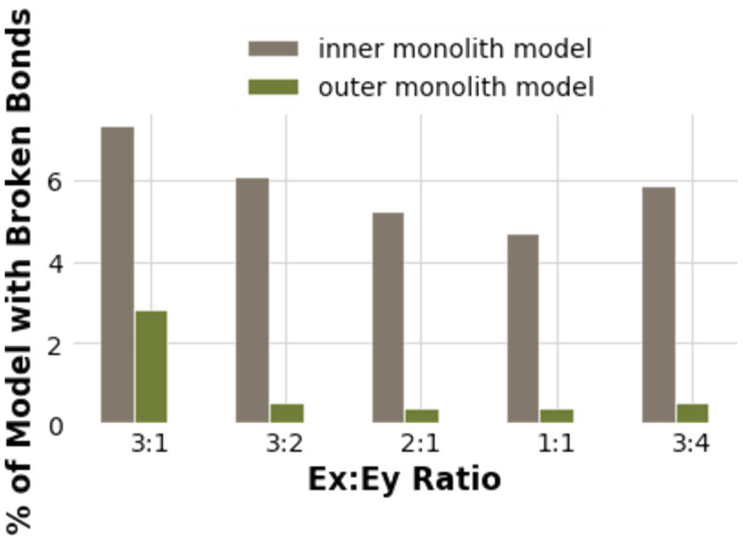

Fig. 9. Number of broken bonds in 0.08 mm node spacing inner monolith model with various E_x: E_y ratios.

Effect of Linear Power Rating

As seen in the base case, Figure 10 shows that the anisotropic model continually predicted higher levels of damage than the isotropic model. Notably, the outer monolith anisotropic model predicts crack extension into the composite at a lower linear power than the isotropic model, at 27 kW m^{-1}, as shown by the circled areas in Figure 11b.

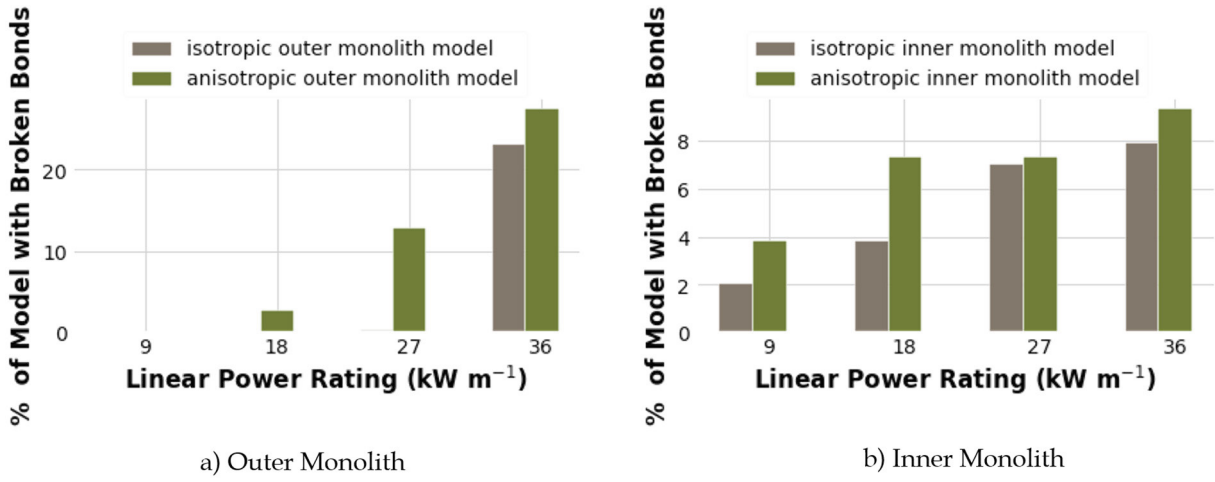

Fig. 10. Effect of fuel linear power rating on the number of bonds broken in 0.08 mm node spacing outer monolith model.

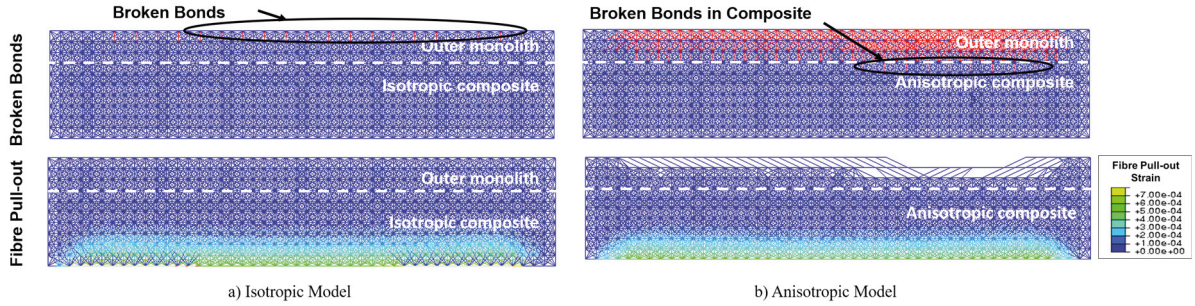

Fig. 11. Broken bonds, top (red) and fibre pull-out strain (bottom) in outer monolith duplex isotropic and anisotropic models at a linear power rating of 27 kW m^{-1} (0.08 mm node spacing).

At the same linear power rating, the inner monolith anisotropic model predicted partial delamination of the monolith-composite interface, while even at 36 kW m^{-1} the isotropic model did not indicate any delamination as shown in Figure 12.

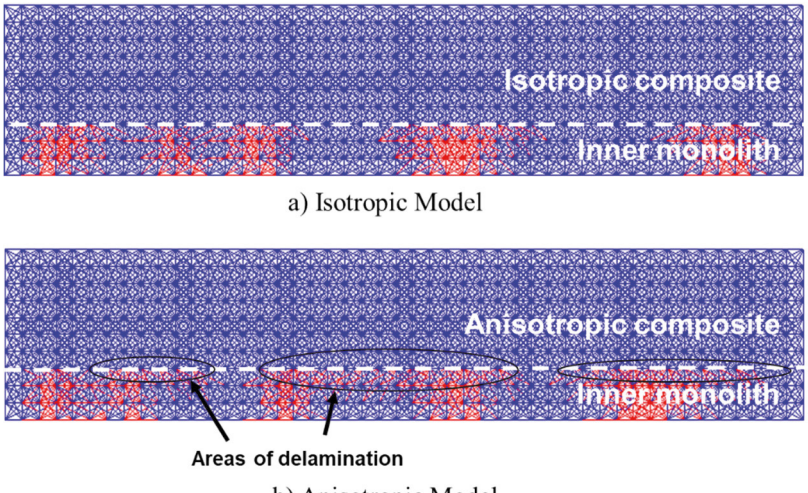

Fig. 12. Damage seen (broken bonds in red) in inner monolith duplex isotropic and anisotropic models at a linear powering rating of 27 kW m^{-1} modelled with 0.08 mm node spacing.

Effect of Thermal Conductivity

For both the isotropic and anisotropic models, a higher thermal conductivity led to less damage in the clad (as shown in the number of cracks and magnitude of fibre pull-out as seen in Figure 13). Additionally, the anisotropic model continued to predict higher levels of damage than the isotropic model (not shown).

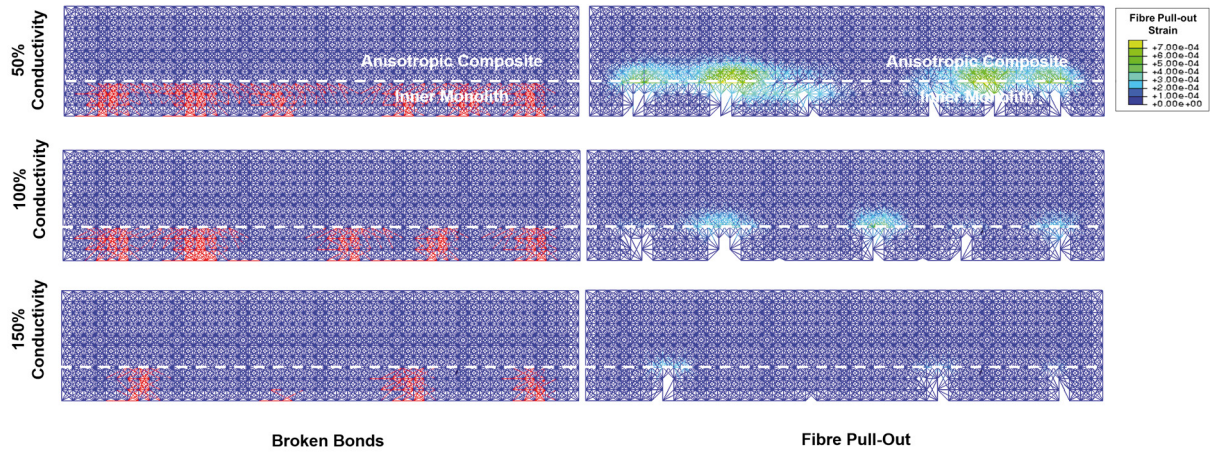

Fig. 13. Effect of thermal conductivity on anisotropic model output in model with 0.08 mm node spacing. Broken bonds on left in red and fibre pull-out strain on right according to key.

4. Discussion

The results of this work agree with wider literature that suggests an duplex model with outer monolith to provide a hermetic seal is the best architecture for a SiC-SiC clad [3, 8]. This is reflected in the low levels of damage and lack of damage propagation seen in the outer monolith model under most of the analysed conditions, (except high linear power >27 kW m^{-1}). Thus, the findings in this work suggest that clad hermicity is retained due to monolith integrity remaining intact.

While some damage was seen in the outer monolith described in the model in Figure 8, the compressive hoop stress that occurs in the outer region of clad prevents this damage growing into a crack. It is surprising that this initial damage occurs since the dominant stresses in the outer region of the cladding, the hoop and axial stresses, are compressive after approximately a year of reactor operation [12], as a result of swelling. Thermomechanical modelling by a number of authors show that the removal of thermal stress (as a result of cooling the reactor) will increase the compressive hoop and axial stress fields. Since switching off the reactor results in rapid cladding cooling, the magnitude of the compressive hoop and axial stress fields will also increase suddenly. According to Poisson's ratio, these compressive stresses may induce a tensile load in the radial direction of the cladding. As the outer free surface experiences the highest compressive stresses, the induced radial tensile stress would be greatest in this direction. Thus the breaking of radial bonds at the outer surface may be a way of releasing the stored elastic strain energy from the high instantaneous stress[1].

Overall, the anisotropic model predicts increased levels of damage to both duplex architectures tested compared with the isotropic model; this suggests that anisotropy increases the magnitude of the tensile hoop field present in the inner monolith and reduces the magnitude of the compressive hoop field found in the outer monolith. This agrees with the findings of Singh et al. [12], whose sensitivity study showed that a relative (25%) increase in circumferential modulus increased the magnitude of hoop stresses (by 15%) at the clad inner surface. Hence, it could be considered that a 2D anisotropic model is analogous to increasing the relative stiffness in one direction as compared to the isotropic case. The notably different levels of damage observed in the results of the anisotropic and isotropic models indicate that considering anisotropy is significant when attempting to model cracks in the r-θ plane of the cladding.

In the fibre pull-out results, pull-out strain is only seen in the inner region of the clad (when an outer monolith is present). This is because the tensile strain field in the inner region of the clad exceeds the PLS of the composite.

[1] Due to the nature of the peridynamic mesh, it is assumed that several bonds must break to create a free surface where we consider surface

The results of the inner monolith model reflect results seen by other authors [5, 8]. As shown in Figure 7, the high tensile inner region of the clad results in cracking of the monolith. No broken bonds are found in the composite because the stress fields in the remainder of the clad either have insufficient tensile stresses or are compressive and consequently the composite is not strained beyond its elastic limit.

Interface

This work uses a strain-compatibility treatment (assuming insignificant slippage at the material interfaces) of the composite-monolith interface which is concurrent with the work of other authors modelling SiC-based clad [8]. This is a suitable representation of the interface as the monolith is chemically bonded to the composite as a result of the CVD process.

Contributions to Crack Arrest at Monolith-Composite Interfaces

In the work of several groups [6, 7, 8], discontinuous changes in the axial, radial and hoop stresses are found at the monolith-composite interfaces. Compared with a composite at the same position in the clad, inner monoliths are under higher tensile stresses. Thus, there is a drop in tensile stress and crack driving force in the composite region of an inner monolith duplex design; this contributes to the consistent crack arrest at the composite-monolith interface, which is seen when an inner monolith was modelled.

The second contributor to crack arrest is the composite's increased toughness. In real SiC-SiC samples composite microcracking, fibre pull-out and friction in the carbon interphase contribute to dissipating the elastic energy stored due to the tensile stress field developed within the clad. However, only fibre pull-out and matrix microcracking are captured in this model as friction would require discretisation of the fibre, matrix and interphase. Matrix microcracking is captured in the SiC-SiC stress-strain curve by the onset of non-elastic strain, when load is transferred to fibres, though it is not explicitly visualised in the composite of this model. As microcracked regions of matrix will strain fibres locally, the position of matrix microcracking can be inferred by the location of fibre pull-out strain in the model presented.

Effect of Modelling Tubular Specimen as a Rectangular Sample

Approximating a tubular section of clad as a rectangle is a suitable approximation to make in this work because the size of clad modelled is a 0.8 mm thick clad of outer radius 4.8 mm, which is aligned with the dimensions of clad test specimens measured by a number of groups [10]. An 1/8th section of clad would have an outer edge measuring 3.77 mm and inner edge measuring 3.14 mm, hence for a rectangular model, the bottom edge is only 20% larger than it should be, and consequently the crack patterns displayed will have minimal distortion compared with using a polar geometry.

Symmetry of Specimen

In this work, boundary conditions on the left and right edges of the model prevent cracks from growing in those regions so cracks close to this region may not display behaviour representative of material behaviour in the bulk. As a section of the clad is modelled it is anticipated that these results would have a degree of rotational symmetry to be able to describe cracks across the r-θ direction of the clad.

Shape of Crack Patterns

There was a greater tendency for monolith cracks in the anisotropic model to branch compared to the isotropic model (Figure 7), indicating more powerful reflective stress waves are generated in the monolith [27]. The greater stress wave reflection is due to: a greater stress discontinuity at the composite-monolith interface and different acoustic impedances in the isotropic vs anisotropic composite [28].

Plane Strain Assumptions

In this work, the LWR simulations assumed a plane strain stress state. This is because the r-θ section of the clad would be constrained by a material (axial length of cladding) above and below the plane being visualised, hence plane strain is a better representation than plane stress. While the crack formation in the axial direction is not considered in this model, other works [6, 7, 8, 12] indicate that the axial and hoop stresses are of the same order of magnitude ($\sim x10^1$ MPa in a fully SiC-SiC model), the radial stresses are much lower ($\sim x10^0$ MPa), so it is expected that the general trends and findings of this work would have similar implications for axial crack growth and damage, (although any interactions of the hoop and axial cracks are not captured here).

E_x: E_y Ratio

Figure 9 shows that levels of damage (broken bonds) in the both duplex monolith models decreased as the ratio of elastic moduli decreased, with levels of fibre pull-out in the composite remaining roughly constant. When cladding architectures were modelled at 0.08 mm node spacing, the maximum level of damage observed in both the inner and outer monolith models occurred at the E_x: E_y ratio obtained from the original RUS data, though simulations at a finer mesh size show that this damage is insufficient to nucleate a crack.

In their thermomechanical modelling work, Singh et al. find that increasing the anisotropy of the SiC-SiC tubing (by increasing the hoop elastic modulus, while holding the axial and radial moduli constant) increases the magnitude of the hoop stress that developed in their simulations. Hence, the trends observed in Figure 9 can likely be explained by the fact that decreasing the ratio of E_x: E_y reduces the relative stiffness of the E_x direction, which would reduce the stress gradient across the clad, resulting in a lower calculated strain and fewer broken bonds.

Damage in the outer monolith has ramifications for the monolith's ability to act as a barrier to hydrothermal corrosion; cracking would provide a higher surface area for corrosion and a pathway for corrosive species to ingress into the clad. At the range of E_x: E_y ratios explored in this work, the outer monolith remained hermetic under the operating conditions simulated.

The fibre winding direction plays a significant role in determining SiC-SiC tubing's elastic properties [3]. Since damage is more prevalent in composite architectures that result in large differences in elastic properties in each orthogonal direction, optimising the fibre winding angle to reduce the difference in elastic properties could reduce the susceptibility of an outer monolith duplex clad to damage.

At all E_x: E_y ratios tested, cracking in the inner monolith was substantial, which would destroy any hermetic effect which an inner monolith design was supposed to confer.

Effect of Linear Power Rating

Both the isotropic and anisotropic model were sensitive to the fuel's linear power rating, though the anisotropic model continued to predict higher levels of cracking and monolith damage, and also lower levels of fibre pull-out. High linear powering ratings increase the temperature gradient across the clad. Of the four contributors to the clad stress state, the temperature gradient affects the swelling strain and thermal strain the most strongly. A higher temperature gradient causes the difference in swelling and thermal expansion of the outer and inner regions to be larger. Thus, upon cooling of the clad during refuelling, there is a larger change in the magnitude of the clad stress state, leading to increased damage. This effect was also seen in the work of Li et al. [6]. Modelling cladding crack behaviour at various linear power ratings is consequential because different sections of the clad experience different linear power ratings as a result of their position in the fuel rod assembly [6].

Effect of Thermal Conductivity

Thermal conductivity is a particularly important parameter to consider as it reduces over the lifetime of the clad due to the formation of irradiation-induced point defects [6]. Thermal conductivity affects the clad stress-state in a similar manner to linear power rating. A higher thermal conductivity results in a lower temperature gradient across the clad, decreasing the thermal strain and swelling strain gradient across the clad. Hence the drivers for damage in models with different thermal conductivities were the same as the drivers for models with different power ratings.

5. Conclusions

This work found that:

- No damage was predicted in a fully composite cladding model with anisotropic elastic properties – this differs to previous findings of Haynes et al. [10].
- Higher levels of damage were predicted in duplex cladding models with an anisotropic composite compared with duplex cladding models with an isotropic composite.
- The anisotropic model predicts damage to occur in both inner and outer monolith models during the cooling of the reactor, when the thermal strain gradient decreases.
- The damage level predicted by the anisotropic model is the most sensitive to linear power rating, but is also sensitive to high levels of orthotropic anisotropy, linear power rating and thermal conductivity.
- In the outer monolith duplex models at linear power rating 18 kW m^{-1}, damage initiated in the monolith at the start of the refuelling outage was found to breach 18% of the monolith but was not predicted to propagate further into the monolith for either the anisotropic or isotropic composite models.

Acknowledgements

Ms Bamgboye wishes to thank Professor Koroush Shirvan for his assistance and support during her time at the Massachusetts Institute of Technology.

Dr Haynes acknowledges funding from the UK Engineering and Physical Sciences Research Council (EPSRC) under grant EP/S01702X/1.

References

[1] S. J. Zinkle et al. "Accident tolerant fuels for LWRs: A perspective". In: *Journal of Nuclear Materials* 448.1-3 (2014), pp. 374–379. issn: 00223115. doi: 10.1016/j.jnucmat.2013.12.005.

[2] Kurt A. Terrani. *Accident tolerant fuel cladding development: Promise, status, and challenges*. 2018. doi: 10.1016/j.jnucmat.2017.12.043.

[3] T Koyanagi et al. *Handbook of LWR SiC|SiC Cladding Properties-Revision 1*. Tech. rep. 2018.

[4] Alexander James Mieloszyk. "Assessing thermo-mechanical performance of ThO and SiC clad light water reactor fuel rods with a modular simulation tool". In: (2015). url: https://dspace.mit.edu/handle/1721.1/103660?show=full.

[5] J. G. Stone et al. "Stress analysis and probabilistic assessment of multi-layer SiC-based accident tolerant nuclear fuel cladding". In: *Journal of Nuclear Materials* 466 (2015), pp. 682–697. issn: 00223115. doi: 10.1016/j.jnucmat.2015.08.001.

[6] Wei Li and Koroush Shirvan. "Finite element analysis of the SiC/SiC composite clad deformation in the presence of spacer grids". In: *Annals of Nuclear Energy* (2019). issn: 18732100. doi: 10.1016/j.anucene.2019.107114.

[7] Valentina Angelici Avincola, Pierre Guenoun, and Koroush Shirvan. "Mechanical performance of SiC three-layer cladding in PWRs". In: *Nuclear Engineering and Design* 310 (2016), pp. 280–294. issn: 00295493. doi: 10.1016/j.nucengdes.2016.10.008.

[8] Youho Lee, Hee Cheon NO, and Jeong Ik Lee. "Design optimization of multi-layer Silicon Carbide cladding for light water reactors". In: *Nuclear Engineering and Design* 311 (2017), pp. 213–223. issn: 00295493. doi: 10.1016/j.nucengdes.2016.11.016.

[9] L. H. Ford, N. S. Hibbert, and D. G. Martin. "Recent developments of coatings for GCFR and HTGCR fuel particles and their performance". In: *Journal of Nuclear Materials* 45.2 (1972), pp. 139–149. issn: 00223115. doi: 10.1016/0022-3115(72)90181-X.

[10] T. A. Haynes, D. Shepherd, and M. R. Wenman. "Preliminary modelling of crack nucleation and propagation in SiC/SiC accident-tolerant fuel during routine operational transients using peridynamics". In: *Journal of Nuclear Materials* 540 (2020), p. 152369. issn: 00223115. doi: 10.1016/j.jnucmat.2020.152369. url: https://doi.org/10.1016/j.jnucmat.2020.152369.

[11] G. M. Jacobsen et al. "Investigation of the C-ring test for measuring hoop tensile strength of nuclear grade ceramic composites". In: *Journal of Nuclear Materials* (2014). issn: 00223115. doi: 10.1016/j.jnucmat.2014.05.002.

[12] Gyanender Singh, Kurt Terrani, and Yutai Katoh. "Thermo-mechanical assessment of full SiC/SiC composite cladding for LWR applications with sensitivity analysis". In: *Journal of Nuclear Materials* (2018). issn: 00223115. doi: 10.1016/j.jnucmat.2017.11.004.

[13] Erkan Oterkus and Erdogan Madenci. "Peridynamic analysis of fiber-reinforced composite materials". In: *Journal of Mechanics of Materials and Structures* 7.1 (2012), pp. 45–84. issn: 1559-3959. doi: 10.2140/jomms.2012.7.45. url: http://msp.org/jomms/2012/7-1/p03.xhtml.

[14] Wenke Hu, Youn Doh Ha, and Florin Bobaru. "Peridynamic model for dynamic fracture in unidirectional fiber-reinforced composites". In: *Computer Methods in Applied Mechanics and Engineering* (2012). issn: 00457825. doi: 10.1016/j.cma.2012.01.016.

[15] Ali Javili et al. "Peridynamics review". In: *Mathematics and Mechanics of Solids* (2018). issn: 17413028. doi: 10.1177/1081286518803411.

[16] M Ghajari, L Iannucci, and P Curtis. *A Peridynamic Material Model for the Analysis of Dynamic Crack Propagation in Orthotropic Media*. Tech. rep.

[17] Richard W. Macek and Stewart A. Silling. "Peridynamics via finite element analysis". In: *Finite Elements in Analysis and Design* (2007). issn: 0168874X. doi: 10.1016/j.finel.2007.08.012.

[18] Jeremy Trageser and Pablo Seleson. "Bond-based peridynamics: A tale of two Poisson's ratios". In: (2019). doi: 10.31224/OSF.IO/SEV3C.

[19] Q V Le and F Bobaru. "Surface corrections for peridynamic models in elasticity and fracture". In: *Computational Mechanics* 61 (2018), pp. 499–518. doi: 10.1007/s00466-017-1469-1. url: https://doi.org/10.1007/s00466-017-1469-1.

[20] R. Mella and M. R. Wenman. "Modelling explicit fracture of nuclear fuel pellets using peridynamics". In: *Journal of Nuclear Materials* 467 (2015), pp. 58–67. issn: 00223115. doi: 10.1016/j.jnucmat.2015.08.037.

[21] R. Beckmann, R. Mella, and M. R. Wenman. "Mesh and timestep sensitivity of fracture from thermal strains using peridynamics implemented in Abaqus". In: *Computer Methods in Applied Mechanics and Engineering* 263 (2013), pp. 71–80. issn: 00457825. doi: 10.1016/j.cma.2013.05.001. url: http://dx.doi.org/10.1016/j.cma.2013.05.001.

[22] Gyanender Singh et al. "Interlaboratory round robin study on axial tensile properties of SiC-SiC CMC tubular test specimens". In: *International Journal of Applied Ceramic Technology* 15.6 (2018), pp. 1334–1349. issn: 1546542X. doi: 10.1111/ijac.13010. url: http://doi.wiley.com/10.1111/ijac.13010.

[23] T Koyanagi et al. *SiC|SiC Cladding Materials Properties Handbook*. Tech. rep. 2017.

[24] Yutai Katoh et al. "Dimensional stability and anisotropy of SiC and SiC-based composites in transition swelling regime". In: *Journal of Nuclear Materials* 499 (2018), pp. 471–479. issn: 00223115. doi: 10.1016/j.jnucmat.2017.12.009.

[25] Yutai Katoh et al. "Continuous SiC fiber, CVI SiC matrix composites for nuclear applications: Properties and irradiation effects". In: *Journal of Nuclear Materials* 448.1-3 (2014), pp. 448–476. issn: 00223115. doi: 10.1016/j.jnucmat.2013.06.040.

[26] K. A. Terrani et al. "Hydrothermal corrosion of SiC in LWR coolant environments in the absence of irradiation". In: *Journal of Nuclear Materials* 465 (2015), pp. 488–498. issn: 00223115. doi: 10.1016/j.jnucmat.2015.06.019.

[27] Youn Doh Ha, Florin Bobaru, and Youn Doh. "Studies of dynamic crack propagation and crack branching with Studies of dynamic crack propagation and crack branching with peridynamics peridynamics "Studies of dynamic crack propagation and crack branching with peridynamics" (2010). Faculty Publications". In: (2010). doi: 10.1007/s10704-010-9442-4.

[28] Adnan I. O. Zaid. "Stress Waves in Solids, Transmission, Reflection and Interaction and Fractures Caused by Them: State of the Art". In: *International Journal of Theoretical and Applied Mechanics* 1 (2016), pp. 155–164.